Available online at www.sciencedirect.com

ScienceDirect

IFAC PapersOnline CONFERENCE PAPER ARCHIVE

IFAC PapersOnLine 58-27 (2024) 61–66

Act-and-Wait Strategy for Mitigating the Effect of Latency in Remote Driving

Xunbi A. Ji *, **Kevin van den Boom** **, **Nathan van de Wouw** **, and **Gábor Orosz** *,***

* *Department of Mechanical Engineering, University of Michigan, Ann Arbor, MI 48109, USA (e-mail: xunbij@umich.edu, orosz@umich.edu)*

** *Department of Mechanical Engineering, Eindhoven University of Technology, Eindhoven, 5600 MB, The Netherlands (e-mail: k.v.d.boom@student.tue.nl, n.v.d.wouw@tue.nl)*

*** *Department of Civil and Environmental Engineering, University of Michigan, Ann Arbor, MI 48109, USA*

Abstract: In this paper, we demonstrate the detrimental effects of latency in remote driving with an example of straight-path following. To address the instability and performance degradation caused by the latency in the remote driving control loop, we propose to use an act-and-wait strategy on top of the existing controller. This strategy can potentially stabilize the system under large latency using the original control gains, and achieve dead-beat control with modified control gains. Stability and performance analysis is conducted for the act-and-wait strategy to provide insights on modulating the control input under large latency.

Keywords: Remote driving, act-and-wait control, stability analysis, end-to-end latency

1. INTRODUCTION

Recently, remote driving has become an appealing topic due to developments of wireless communication technologies. It is an important supplement to automated driving, and can be integrated into self-driving vehicles (Kang et al., 2018). As illustrated in Fig. 1(a), a remotely-driven (teleoperated) vehicle transmits/receives information through wireless communication networks to/from the remote operator, which is either a robot or a human driver located in a remote center. The remote operator may take over the vehicle and ensure safety when there is a failure of the on-board autonomy algorithms or a critical (e.g., health-related) situation occurs for the human driver. Other advantages include the possibility of offloading computational power from the vehicle to a remote server and making a driverless car, equipped with the right sensors and actuators, to operate without having onboard autonomy software.

One big challenge of remote driving is that the communication networks between the operator and the vehicle introduce significant delays in delivering the information, e.g., video streaming, sensor data, actuation commands (Liu et al., 2017; Yang and Yang, 2020). The communication delays may vary, depending on the location, network congestion and even the weather. In case of a human operator at the remote center, additional reaction time delay appears which could be different per operator and change under different situations. Even with automatic control, the perception unit also can introduce nonnegligible delay (Oliveira et al., 2016; Pendleton et al., 2017; Fayyad et al., 2020) and vehicles may possess significant actuation delays (Ji et al., 2021). These delays cannot

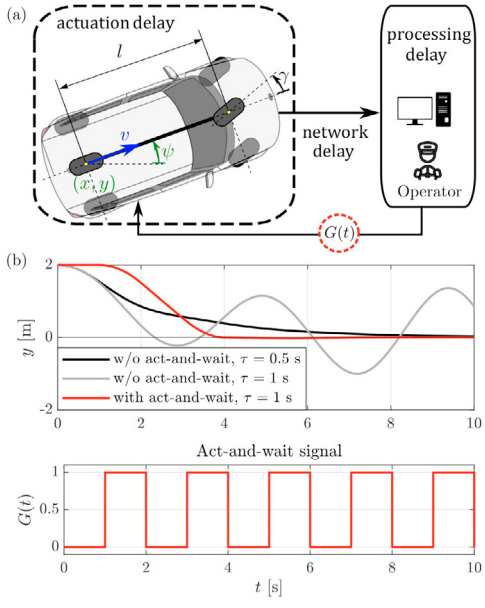

Fig. 1. (a) The framework of remote driving with delays. (b) Using act-and-wait strategy on top of existing remote operator to stabilize the system under large delay. Top: Simulations of a vehicle following a straight line $y = 0$ under different delays. The nominal control gains chosen for delay $\tau = 0.5$ s (black) lose stability when the delay increases to 1 s (grey). After applying the act-and-wait signal on top the nominal controller (without changing the control gains), the system becomes stable again. Bottom: The periodic act-and-wait signal used in the simulation.

10.1016/j.ifacol.2024.10.300

simply be eliminated and this requires the system to be robust against (changes in) the delays.

To address the negative effects of the overall delay in the remote-driving control loop, some researchers have been trying to reduce the delays (Willars et al., 2021; Brunello et al., 2021). Others tried to work with the inevitable delay. For example, a predictive display system (Sharma and Rajamani, 2024) was developed to compensate the communication latency in teleportation using model-based extended Kalman filter. The Smith predictor (Najafi, 2021) can be used to achieve delay-free performance if the delay and the plant model are accurately known. Intermittent control (Gawthrop and Wang, 2007; Liu et al., 2023) reduces the infinite-dimensional time delay system to finite dimension, by utilizing predictive control intermittently. Other methods include optimal control (Cacace et al., 2016) and H_∞ control (Zhong, 2006; Ma et al., 2023). These methods result in standalone controllers and are not applicable on top of an existing automatic controller or on a human operator.

In this work, we propose to use act-and-wait algorithms (Insperger, 2006; Gawthrop, 2010; Michiels and Zhou, 2020; Zhou et al., 2021). Compared to the mitigation methods mentioned above, act-and-wait algorithms can be directly implemented as an add-on to the existing controller. By switching the control on and off periodically, the original infinite-dimensional delay system can be reduced to a finite-dimensional system. As illustrated in Fig. 1(b), when the act-and-wait signal $G(t)$ is used on top of the remote operator the systems achieves supreme control performance. For large enough delay, the original controller may lose stability (gray curve). With the act-and-wait algorithm applied on the same controller (same control gains), the system converges to the steady state much faster (red curve). Besides addressing the delays in the control loop, one also needs to evaluate the robustness of the controller against the changes in the delay. Methods for examining the stability and the performance of time delay systems are well established (Insperger and Stépán, 2011) and these can be generalized to study the robustness of stability against changes in system parameters, including the delay.

The main contributions of this work are summarized as follows. First, the effect of the delay and velocity on remote driving is studied analytically in terms of stability and convergence rate without and with the act-and-wait algorithm. Second, we derive the robustness coefficient that represents how much delay the system may tolerate before losing stability. Third, the advantages of using the act-and-wait algorithm on top of a nominal controller are demonstrated.

The rest of the paper is organized as follows. In Section 2, we perform stability analysis on a dimensionless model and derive a closed-form expression for the control gains that guarantee the fastest-convergence. In Section 3, we introduce the act-and-wait algorithm and derive the deadbeat control gains. In Section 4 we demonstrate the effects of the delay and velocity, as well as the advantage of applying the act-and-wait algorithm, through numerical simulations. We summarize the results and discuss the future directions in Section 5.

2. REMOTE DRIVING UNDER LATENCY

In this work, we consider a scenario of a remote-controlled vehicle following a straight line, for example, a lane-changing maneuver guided by the remote operator. Moreover, we assume that the overall latency in the control loop mostly comes from the delays prior to the controller, i.e., uplink latency due to the video streaming and the image processing/perception delay. For a static controller, the location of delay in the control loop only affects the simulation results via the initial history, while the stability is only influenced by the magnitude of the overall delay.

We consider the kinematic vehicle model (Qin et al., 2022)

$$\begin{aligned} \dot{x}(t) &= v\cos(\psi(t)),\\ \dot{y}(t) &= v\sin(\psi(t)),\\ \dot{\psi}(t) &= \frac{v}{l}\tan(\gamma(t)), \end{aligned} \tag{1}$$

shown in Fig. 1(a) with controller

$$\gamma(t) = \arctan\big(-k_y y(t-\tau) - k_\psi \psi(t-\tau)\big), \tag{2}$$

aiming to stabilize the rectilinear motion $y \equiv 0$, $\psi \equiv 0$. Here (x, y) are the coordinates of the center of the rear axle, ψ is the yaw angle, and γ is the steering control input. The parameters are the longitudinal velocity v, the wheelbase, l, the time delay τ, and the control gains k_y, k_ψ.

We first nondimensionalize the system using the dimensionless quantities $\hat{t} = tv/l$, $\hat{\tau} = \tau v/l$, $\hat{y} = y/l$, $\hat{x} = x/l$, $\hat{\psi} = \tilde{\psi}$ which yields

$$\begin{aligned} \hat{x}'(\hat{t}) &= \cos(\hat{\psi}(\hat{t})),\\ \hat{y}'(\hat{t}) &= \sin(\hat{\psi}(\hat{t})),\\ \hat{\psi}'(\hat{t}) &= -l\,k_y \hat{y}(\hat{t}-\hat{\tau}) - k_\psi \hat{\psi}(\hat{t}-\hat{\tau}), \end{aligned} \tag{3}$$

where the prime represents derivative with respect to the dimensionless time $\hat{t}$. Then we linearize the system around the steady state $\hat{x}^* \equiv \hat{t} + x(0)$, $\hat{y}^* \equiv 0$, $\hat{\psi}^* \equiv 0$. By defining the perturbations $\tilde{x} = \hat{x} - x^*$, $\tilde{y} = \hat{y} - y^*$, $\tilde{\psi} = \hat{\psi} - \psi^*$, we obtain the linear and dimensionless system

$$\begin{aligned} \tilde{x}'(\hat{t}) &= 0,\\ \tilde{y}'(\hat{t}) &= \tilde{\psi}(\hat{t}),\\ \tilde{\psi}'(\hat{t}) &= -l\,k_y \tilde{y}(\hat{t}-\hat{\tau}) - k_\psi \tilde{\psi}(\hat{t}-\hat{\tau}). \end{aligned} \tag{4}$$

The stability of lateral dynamics is given by the characteristic equation

$$\lambda^2 + k_\psi e^{-\lambda\hat{\tau}}\lambda + k_y l e^{-\lambda\hat{\tau}} = 0, \tag{5}$$

that is obtained from the second and third rows of (4). The state $\hat{y}^* \equiv 0$, $\hat{\psi}^* \equiv 0$ is exponentially stable if and only if all characteristic roots of (5) have negative real parts, i.e., $\mathrm{Re}(\lambda_i) < 0, i = 1, 2, \ldots$. Substituting $\lambda = 0$ yields the stability boundary

$$l\,k_y = 0, \tag{6}$$

and using $\lambda = \mathrm{j}\omega$, $\omega > 0$ results in the stability boundary

$$\begin{aligned} k_\psi &= \omega \sin\omega\hat{\tau},\\ l\,k_y &= \omega^2 \cos\omega\hat{\tau}, \end{aligned} \tag{7}$$

which is parameterized by the angular frequency ω. The stability boundaries related to different levels of the dimensionless delay are shown in Fig. 2(a). The stable region shrinks as the dimensionless delay $\hat{\tau}$ increases. Since $\hat{\tau} = v\tau/l$, increasing the velocity or increasing the actual delay in the system has the same effect on stability.

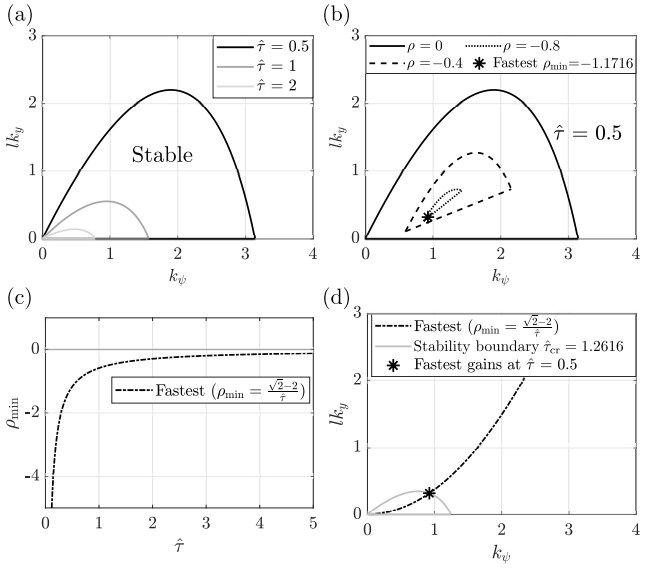

Fig. 2. (a) Stability boundaries for different dimensionless delays $\hat{\tau}$. (b) Performance curves for different convergence rates ρ values when $\hat{\tau} = 0.5$. (c) The fastest convergence rate $\rho_{\min}$ as a function of $\hat{\tau}$. (d) The control gains which give $\rho_{\min}$ are plotted as the black dashed-dotted curve. This curve intersects the stability boundary of $\hat{\tau}_{\rm cr} = 1.2616$ (grey solid curve) when $\hat{\tau} = 0.5$.

The real parts of the characteristic roots indicate how fast the system converges to the steady state given an initial error. By substituting $\lambda = \rho + \mathrm{j}\omega, \rho < 0, \omega \geq 0$ into the characteristic equation (5), one can solve for the curves with respect to each ρ. For $\omega = 0$, we have

$$l\,k_y = -\rho \mathrm{e}^{\rho\hat{\tau}}(\rho + k_\psi \mathrm{e}^{-\rho\hat{\tau}}), \tag{8}$$

and for $\omega > 0$, we obtain

$$\begin{aligned} k_\psi &= -\mathrm{e}^{\rho\hat{\tau}}\big(\rho^2 - \omega^2\big)\sin(\omega\hat{\tau}) + 2\rho\omega\cos(\omega\hat{\tau})\big)/\omega, \\ l\,k_y &= -\mathrm{e}^{\rho\hat{\tau}}\big((\rho^2 - \omega^2)\cos(\omega\hat{\tau}) - 2\rho\omega\sin(\omega\hat{\tau})\big) - k_\psi\rho. \end{aligned} \tag{9}$$

These so-called performance curves are plotted for different ρ values in Fig. 2(b) when $\hat{\tau} = 0.5$. The curves (9) are parameterized by the angular frequency ω such that $\omega \to 0$ locates at the left corner of the performance domain.

Indeed, the performance curve for $\rho = 0$ is the stability boundary. As the ρ decreases, the region enclosed by performance curves shrinks and eventually disappears at $\rho_{\min}$, which gives the fastest convergence rate. This happens when the slope of (8) and the slope of (9) for $\omega \to 0$ become equal. This yields

$$\rho_{\min} = \frac{\sqrt{2} - 2}{\hat{\tau}}, \tag{10}$$

which only depends on the dimensionless delay $\hat{\tau}$, as depicted in Fig. 2(c). Substituting this into (9) and using $\omega \to 0$, we obtain the gains corresponding to $\rho_{\min}$ as functions of $\hat{\tau}$:

$$\begin{aligned} k_{\psi,\min} &= \frac{p}{\hat{\tau}}, \\ l\,k_{y,\min} &= \frac{q}{\hat{\tau}^2}, \end{aligned} \tag{11}$$

where $p = -\mathrm{e}^{\sqrt{2}-2}\left(2 - 2\sqrt{2}\right)$ and $q = \mathrm{e}^{\sqrt{2}-2}\left(10\sqrt{2} - 14\right)$. This is plotted as a dotted-dashed curve in Fig. 2(d).

This curve intersects all stability boundaries, which means that the fastest-convergence gains designed for a given delay $\hat{\tau}$ are located on the stability boundary of another (larger) delay $\hat{\tau}_{\rm cr}$. We can derive the analytical relationship between $\hat{\tau}$ and $\hat{\tau}_{\rm cr}$ by equating (7) and (11):

$$\begin{aligned} k_{\psi,\min}(\hat{\tau}) &= k_\psi(\omega_{\rm cr}, \hat{\tau}_{\rm cr}), \\ l\,k_{y,\min}(\hat{\tau}) &= l\,k_y(\omega_{\rm cr}, \hat{\tau}_{\rm cr}), \end{aligned} \tag{12}$$

which yields

$$\begin{aligned} \omega_{\rm cr} &= \frac{g}{\hat{\tau}}, \\ \hat{\tau}_{\rm cr} &= \frac{1}{g}\sin^{-1}\left(\frac{p}{g}\right)\hat{\tau} \approx 2.5232\,\hat{\tau}, \end{aligned} \tag{13}$$

where $g = \sqrt{\frac{p^2 + \sqrt{p^4 + 4q^2}}{2}}$. Observe that the coefficient giving the linear relationship between $\hat{\tau}$ and $\hat{\tau}_{\rm cr}$ does not depend on any parameter. In Fig. 2(d), we mark the gains that give the fastest convergence for $\hat{\tau} = 0.5$ (black star), which is indeed located on the stability boundary for $\hat{\tau}_{\rm cr} = 2.5232\hat{\tau} \approx 1.2616$ (gray curve).

These results quantify the robustness of the fastest-convergence gains against the change of the dimensionless delay $\hat{\tau} = v\tau/l$, i.e., against the change of the velocity v and actual delay τ in the remote-driving control loop. If the fastest-convergence gains are chosen, the system can maintain stability even when either the velocity or the delay or their product increases up to 2.5 times. Note that, in case of human operator, the fastest-convergence gains may not be achieved and stability may not be guaranteed for larger delays. Below we introduce the act-and-wait strategy to mitigate the effect of the delay and improve the performance.

3. REMOTE DRIVING WITH ACT-AND-WAIT

In this section, we describe the act-and-wait control strategy, and utilize it in the context of the remote driving task. Control gains are derived analytically to achieve dead-beat (DB) transient performance even in case of large delays. The robustness of the DB gains are also examined against the change of delay and/or velocity.

3.1 Act-and-wait algorithm

Consider a generic linear system with feedback control based on the delayed state

$$\begin{aligned} \dot{X}(t) &= \mathbf{A}X(t) + \mathbf{B}U(t), \\ U(t) &= G(t)\mathbf{K}X(t - \tau), \end{aligned} \tag{14}$$

where X is the state, U is the control input, $\mathbf{K}$ contains the control gains, and $G(t)$ is defined as

$$G(t) = \begin{cases} 0, & \text{if } 0 \leq (t \bmod T) < t_{\rm w}, \\ 1, & \text{if } t_{\rm w} \leq (t \bmod T) < T. \end{cases} \tag{15}$$

Here, $T = t_{\rm w} + t_{\rm a}$ is the period, $t_{\rm w}$ and $t_{\rm a}$ are the waiting and acting time. The closed-loop dynamics are given by

$$\dot{X}(t) = \mathbf{A}X(t) + G(t)\mathbf{A}_\tau X(t - \tau), \tag{16}$$

where $\mathbf{A}_\tau = \mathbf{BK}$.

With the assumptions $t_{\rm w} > \tau$ and $0 < t_{\rm a} < t_{\rm w}$, one can convert the continuous-time system (16) into a discrete-time map linking the state at the beginning of the act-and-wait interval to the state at the end of that interval:

$$X(kT + T) = \Phi X(kT), \quad k = 0, 1, ..., \tag{17}$$

where the monodromy matrix Φ is derived as

$$\Phi = e^{\mathbf{A}T} + \int_{t_\mathrm{w}}^{T} e^{\mathbf{A}(T-s)}\mathbf{A}_\tau\, e^{\mathbf{A}(s-\tau)}\mathrm{d}s. \tag{18}$$

The stability of the discrete-time linear system (17) is determined by the eigenvalues of the monodromy matrix Φ, also known as the characteristic multipliers.

3.2 Act-and-wait steering control

In the remote-driving application (1), (2), we apply the act-and-wait signal $G(t)$ to the argument of the "arctan" function in the controller. We further assume $t_\mathrm{w} = \tau$ and use the act-wait ratio $a = t_\mathrm{a}/t_\mathrm{w}$, $0 < a \le 1$, to tune the act-and-wait signal. The closed-loop dynamics becomes

$$\begin{aligned} \dot{x}(t) &= v\cos(\psi(t)),\\ \dot{y}(t) &= v\sin(\psi(t)),\\ \dot{\psi}(t) &= \frac{v}{l}G(t)\big(-k_y y(t-\tau) - k_\psi \psi(t-\tau)\big). \end{aligned} \tag{19}$$

After nondimensionalization and linearization, the stability of the lateral dynamics (given by the last two rows in (19)) are characterized by the monodromy matrix

$$\Phi = e^{\mathbf{A}\widehat{T}} + \int_{\hat{t}_\mathrm{w}}^{\widehat{T}} e^{\mathbf{A}(\widehat{T}-s)}\mathbf{A}_{\hat{\tau}}\, e^{\mathbf{A}(s-\hat{\tau})}\mathrm{d}s, \tag{20}$$

where $\mathbf{A} = \begin{bmatrix} 0 & 1 \\ 0 & 0 \end{bmatrix}$, $\mathbf{A}_{\hat{\tau}} = \begin{bmatrix} 0 & 0 \\ -l\,k_y & -k_\psi \end{bmatrix}$, $\widehat{T} = (1+a)\hat{\tau}$ and $\hat{t}_\mathrm{w} = \hat{\tau}$. The analytical form of the monodromy matrix is

$$\Phi = \begin{bmatrix} 1 - \dfrac{l\,k_y a^2\hat{\tau}^2}{2} & (a+1)\hat{\tau} - \dfrac{k_\psi a^2\hat{\tau}^2}{2} - \dfrac{l\,k_y a^3\hat{\tau}^3}{6} \\ -l\,k_y\,a\hat{\tau} & 1 - k_\psi\,a\hat{\tau} - \dfrac{l\,k_y a^2\hat{\tau}^2}{2} \end{bmatrix}. \tag{21}$$

The eigenvalues μ_1, μ_2 of this matrix can be obtained analytically and the discrete-time system (17) with $X = [\tilde{y},\, \tilde{\psi}]^\top$ is exponentially stable if and only if $|\mu_1| < 1$ and $|\mu_2| < 1$. As shown by Belyakov and Seyranian (2020), this is equivalent to satisfying inequalities $|\mathrm{tr}(\Phi)| - 1 < \det(\Phi)$ and $\det(\Phi) < 1$, which result in the stability conditions

$$\begin{aligned} k_\psi &< \frac{1}{24}a^3\hat{\tau}^3(l\,k_y)^2 - \frac{1}{2}a\hat{\tau}\,l\,k_y + \frac{1}{2}\hat{\tau}\,l\,k_y + \frac{2}{a\hat{\tau}},\\ k_\psi &> \frac{1}{12}\,a^3\hat{\tau}^3(l\,k_y)^2 + \hat{\tau}\,l\,k_y,\\ l\,k_y &> 0. \end{aligned} \tag{22}$$

The stable regions enclosed by these three boundaries are shown in Fig. 3(a) and (b) for different values of the dimensionless delay $\hat{\tau}$ and different choices of the act-wait ratio a. Comparing these to the chart in Fig 2(a), one may observe that applying the act-and-wait strategy significantly increases the stable region. The stable region still shrinks as $\hat{\tau}$ increases, and it expands as a decreases. Therefore, adjusting the act-and-wait signal could help to stabilize the system under large delay.

Moreover, if $\mu_1 = \mu_2 = 0$, the solution converges to zero after two periods (since $\Phi^2 = \mathbf{0}$), which we refer to as dead-beat (DB) control. The corresponding control gains can be calculated analytically:

$$\begin{aligned} lk_{y,\mathrm{db}} &= \frac{-6a - 6 + 2\sqrt{12a^2+18a+9}}{a^3\hat{\tau}^2},\\ k_{\psi,\mathrm{db}} &= \frac{8a + 6 - 2\sqrt{12a^2+18a+9}}{a^2\hat{\tau}}, \end{aligned} \tag{23}$$

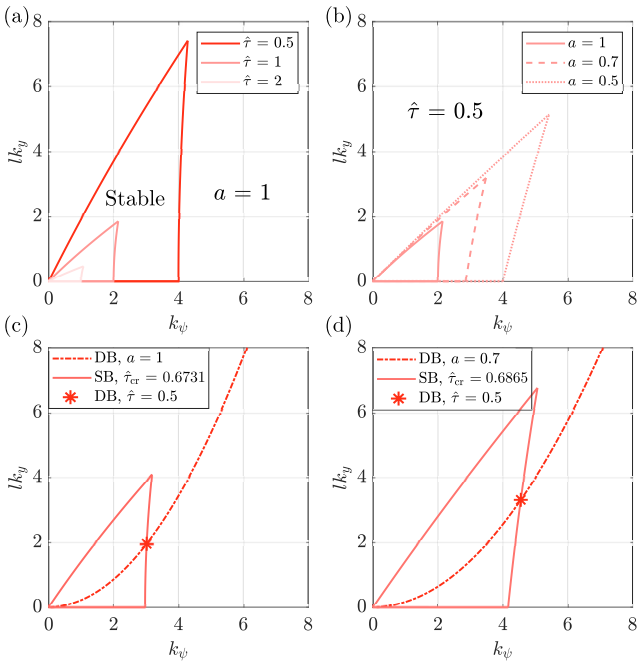

Fig. 3. (a) Stability boundaries for different values of the dimensionless delay $\hat{\tau}$ when $a = 1$. (b) Stability boundaries for different values of the act-wait ratio a when $\hat{\tau} = 1$. (c) The control gains which give the dead-beat (DB) control are plotted as a red dashed-dotted curve for $a = 1$. The DB curve intersects the stability boundary of $\hat{\tau}_{\mathrm{cr}} = 0.6731$ (red solid curve) at $\hat{\tau} = 0.5$. (d) The DB curve (red dashed-dotted curve) for $a = 0.7$ intersects the stability boundary of $\hat{\tau}_{\mathrm{cr}} = 0.6865$ (red solid curve) at $\hat{\tau} = 0.5$.

and these depend on a and $\hat{\tau}$ only. The DB control gains are shown in Fig. 3(c) and (d) as red dashed-dotted curves for $a = 1$ and $a = 0.7$, respectively. Similar to the continuous-time system, these curves intersect the stability boundaries. The DB gains for $\hat{\tau} = 0.5$ are marked by red starts and these are located at the stability boundary of the critical delay value $\hat{\tau}_{\mathrm{cr}}$. However, the relationship between $\hat{\tau}$ and $\hat{\tau}_{\mathrm{cr}}$ now depends on the choice of a.

From (22), the right boundary is given by

$$k_\psi = \frac{1}{24}a^3\hat{\tau}_{\mathrm{cr}}^3(l\,k_y)^2 - \frac{1}{2}a\hat{\tau}_{\mathrm{cr}}l\,k_y + \frac{1}{2}\hat{\tau}_{\mathrm{cr}}l\,k_y + \frac{2}{a\hat{\tau}_{\mathrm{cr}}}. \tag{24}$$

Therefore, substituting (23), we obtain the fourth-order equation

$$\frac{r^2}{3a}\left(\frac{\hat{\tau}_{\mathrm{cr}}}{\hat{\tau}}\right)^4 + \frac{2ar - 2r}{a}\left(\frac{\hat{\tau}_{\mathrm{cr}}}{\hat{\tau}}\right)^2 - (4a+4r)\frac{\hat{\tau}_{\mathrm{cr}}}{\hat{\tau}} + 4a = 0, \tag{25}$$

where $r = 3a + 3 - \sqrt{12a^2+18a+9}$. This can be solved numerically, for $\hat{\tau}_{\mathrm{cr}}/\hat{\tau}$ and the solution is plotted in Fig. 4 as a function of a. The coefficient $\hat{\tau}_{\mathrm{cr}}/\hat{\tau}$ decreases with a, changing from 2 to 1.3463. Recall that this coefficient is a constant around 2.5 for the continuous-time system without act-and-wait, cf. (13). Although the robustness coefficient is smaller, applying act-and-wait greatly increases the absolute stability region and significantly improves the performance. This will be demonstrated in the next section through numerical simulations.

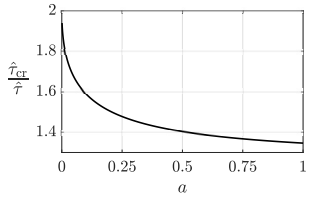

Fig. 4. Robustness coefficient $\hat{\tau}_{\mathrm{cr}}/\hat{\tau}$ as a function of the act-wait ratio a.

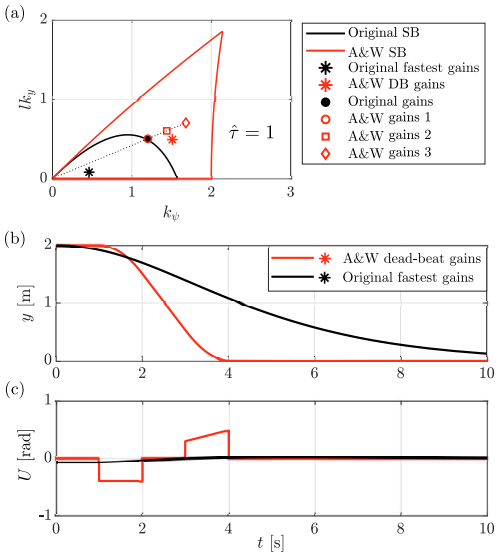

Fig. 5. (a) Stability boundaries and selected control gains for scenarios with and without act-and-wait algorithm shown by red and black colors, respectively. (b) and (c) Simulation results for different choices of control gains with and without act-and-wait algorithms.

4. SIMULATION RESULTS WITH AND WITHOUT ACT-AND-WAIT ALGORITHM

In this section, we simulate nonlinear system (1), (2) and the nonlinear system (19) with different choices of control gains and relate the linear stability charts with the nonlinear behaviors. In the simulation, we use the constant longitudinal velocity $v = 2.5$ m/s, the wheelbase $l = 2.5$ m, and the delay $\tau = 1$ s, which give the dimensionless delay $\hat{\tau} = 1$. For the act-and-wait algorithm, we select $a = 1$ and $t_{\mathrm{w}} = \tau$. This means that the acting period is the same as the waiting period, as well as the delay in the system. Although the system is nonlinear, the effect of the nonlinearity is small as we consider small yaw angles.

First, we compare the performance of the original system without act-and-wait control to the one with act-and wait. In Fig. 5(a), we compare the stable domain of the original system (bounded by the black curves) to that of the system with act-and-wait on the top of the same controller when using $a = 1$ (bounded by the red curves). Observe the significant expansion of the stable domain due to act-and-wait. The black star corresponds to the fastest convergence rate $\rho_{\min} = -0.5858$ for the original controller, and the red star corresponds to the dead-beat control gains for act-and-wait enhanced controller. The lateral error and the control input are shown in Fig. 5(b) and (c), when the "best-performance" gains are chosen in both scenarios. Despite the late start of the

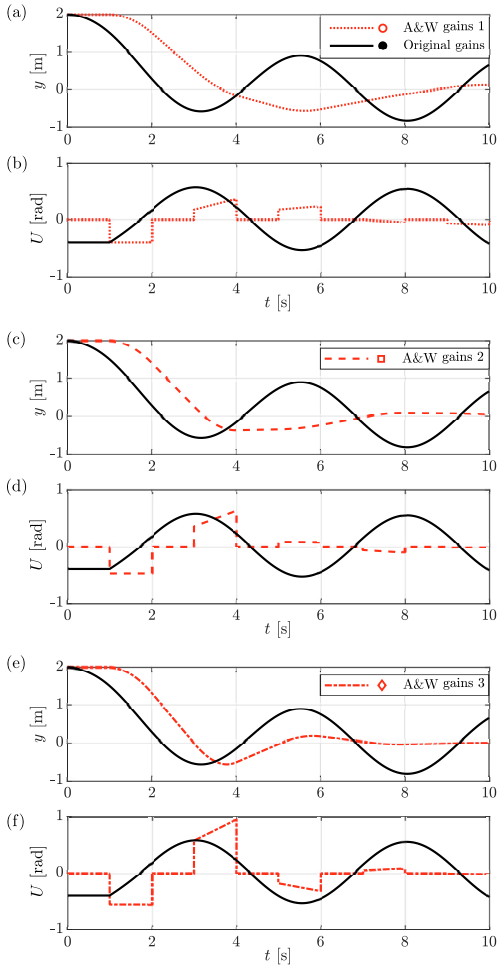

Fig. 6. Simulations when using the act-and-wait algorithm with different amplifications of the control gains. (a)-(b) No amplification of the control gains. (c)-(d) Amplification with coefficient 1.2. (d)-(e) Amplification with coefficient 1.4.

action and the non-smooth control input caused by the waiting periods, the system with act-and-wait algorithm can converge faster. As demonstrated in panel (b), the system converges in 4 seconds (two periods) with the DB gains, while the fastest convergence without act-and-wait takes around 10 seconds.

The system may lose stability for some control gains, see, for instance, the gains marked by the black dot just outside the stability boundary in Fig. 5(a). One can apply act-and-wait on top of the current controller to stabilize the system. Additionally, the final control input can be amplified by multiplying a coefficient to achieve better performance while exploiting the larger stable region under act-and-wait. This is equivalent to increasing control gains along the dotted black line. We amplify the control input by different coefficients 1, 1.2 and 1.4 as indicated by the red circle, square and diamond, respectively. In Fig. 6, we show the simulation results for those three gains with act-and-wait (red curves) and compare the results to the original system without act-and-wait (black curves) to highlight the performance improvements in terms of convergence time. These highlight the benefits of modulating the control signal without changing the original controller, which can potentially be applied on top of a human remote

operator to assist remote driving. Note that the location of the original gains also influences the performance of the algorithm. Thus, to achieve the best performance, it may be necessary to tune the two gains individually.

5. CONCLUSION

We demonstrated the effects of delay in remote driving both analytically and numerically. We proposed to apply the act-and-wait algorithm on top of the original controller to achieve better control performance. We studied the linear stability and the performance in terms of convergence rate for both systems and demonstrated the advantages of using act-and-wait systems under large delays. The "best-performance" control gains, which give the fastest convergence rate and dead-beat control performance, are derived in closed-form as functions of dimensionless delays, i.e., a combination of longitudinal velocity and end-to-end delay in the loop. The robustness coefficient is derived to demonstrate how much change of the dimensionless delay the system can endure before loosing the stability, when the "best-performance" gains are chosen.

With act-and-wait algorithm, the stable region in the parameter space increases while the robustness coefficient decreases. The system with act-and-wait algorithm also converges much faster at its best performance. It means that the act-and-wait could potentially stabilize the system and achieve better control performance, but the performance is also more sensitive to the change of delay and velocity. As future directions, we will improve the act-and-wait algorithm to generate smoother and more realistic input signals and compare the results to other delay mitigation methods. We will apply the act-and-wait algorithm on other maneuvers such as following a curved path. We also plan to study the robustness of using act-and-wait strategy when the delay in the system is unknown.

REFERENCES

Belyakov, A.O. and Seyranian, A.P. (2020). Stability boundary approximation of periodic dynamics. In *1st International Nonlinear Dynamics Conference (NODYCON 2019), Volume I*, 13–23. Springer.

Brunello, D., Johansson, I., Ozger, M., and Cavdar, C. (2021). Low latency low loss scalable throughput in 5g networks. In *93rd IEEE Vehicular Technology Conference (VTC2021-Spring)*, 1–7. IEEE.

Cacace, F., Conte, F., Germani, A., and Palombo, G. (2016). Optimal control of linear systems with large and variable input delays. *Systems & Control Letters*, 89, 1–7.

Fayyad, J., Jaradat, M.A., Gruyer, D., and Najjaran, H. (2020). Deep learning sensor fusion for autonomous vehicle perception and localization: A review. *Sensors*, 20(15), 4220.

Gawthrop, P. (2010). Act-and-wait and intermittent control: Some comments. *IEEE Transactions on Control Systems Technology*, 18(5), 1195–1198.

Gawthrop, P.J. and Wang, L. (2007). Intermittent model predictive control. *Proceedings of the Institution of Mechanical Engineers, Part I*, 221(7), 1007–1018.

Insperger, T. (2006). Act-and-wait concept for continuous-time control systems with feedback delay. *IEEE Transactions on Control Systems Technology*, 14(5), 974–977.

Insperger, T. and Stépán, G. (2011). *Semi-discretization for time-delay systems: stability and engineering applications*, volume 178. Springer.

Ji, X.A., Molnár, T.G., Gorodetsky, A.A., and Orosz, G. (2021). Bayesian inference for time delay systems with application to connected automated vehicles. In *IEEE International Intelligent Transportation Systems Conference (ITSC)*, 3259–3264. IEEE.

Kang, L., Zhao, W., Qi, B., and Banerjee, S. (2018). Augmenting self-driving with remote control: Challenges and directions. In *19th International Workshop on Mobile Computing Systems & Applications*, 19–24.

Liu, B., Liu, T., and Xiao, P. (2023). Dynamic event-triggered intermittent control for stabilization of delayed dynamical systems. *Automatica*, 149, 110847.

Liu, R., Kwak, D., Devarakonda, S., Bekris, K., and Iftode, L. (2017). Investigating remote driving over the lte network. In *9th International Conference on Automotive User Interfaces and Interactive Vehicular Applications*, 264–269.

Ma, X., Wong, P.K., Li, W., Zhao, J., Ghadikolaei, M.A., and Xie, Z. (2023). Multi-objective H_2/H_∞ control of uncertain active suspension systems with interval time-varying delay. *Proceedings of the Institution of Mechanical Engineers, Part I: Journal of Systems and Control Engineering*, 237(2), 335–347.

Michiels, W. and Zhou, B. (2020). On the fixed-time stabilization of input delay systems using act-and-wait control. *Systems & Control Letters*, 146, 104807.

Najafi, M. (2021). Stabilization techniques for large input-delay systems with uncertainty. In *Control Strategy for Time-Delay Systems*, 83–110. Elsevier.

Oliveira, G.L., Burgard, W., and Brox, T. (2016). Efficient deep models for monocular road segmentation. In *IEEE/RSJ International Conference on Intelligent Robots and Systems (IROS)*, 4885–4891. IEEE.

Pendleton, S.D., Andersen, H., Du, X., Shen, X., Meghjani, M., Eng, Y.H., Rus, D., and Ang, M.H. (2017). Perception, planning, control, and coordination for autonomous vehicles. *Machines*, 5(1), 6.

Qin, W.B., Zhang, Y., Takács, D., Stépán, G., and Orosz, G. (2022). Nonholonomic dynamics and control of road vehicles: moving toward automation. *Nonlinear Dynamics*, 110(3), 1959–2004.

Sharma, G. and Rajamani, R. (2024). Teleoperation enhancement for autonomous vehicles using estimation based predictive display. *IEEE Transactions on Intelligent Vehicles*, 9(3), 4456–4469.

Willars, P., Wittenmark, E., Ronkainen, H., Östberg, C., Johansson, I., Strand, J., Lédl, P., and Schnieders, D. (2021). Enabling time-critical applications over 5G with rate adaptation. *White Paper BNEW-21*, 25455.

Yang, Q. and Yang, J.H. (2020). HD video transmission of multi-rotor unmanned aerial vehicle based on 5G cellular communication network. *Computer Communications*, 160, 688–696.

Zhong, Q.C. (2006). *Robust Control of Time-delay Systems*. Springer.

Zhou, B., Michiels, W., and Chen, J. (2021). Fixed-time stabilization of linear delay systems by smooth periodic delayed feedback. *IEEE Transactions on Automatic Control*, 67(2), 557–573.